Topological-Fermi-liquid to quantum-Hall-liquid transitions: *p*-band and *d*-band fermions in an external magnetic field

Yi-Fei Wang[1] and Chang-De Gong[1,2]

[1]*Center for Statistical and Theoretical Condensed Matter Physics, and Department of Physics, Zhejiang Normal University, Jinhua 321004, China*

[2]*National Laboratory of Solid State Microstructures and Department of Physics, Nanjing University, Nanjing 210093, China*

(Received 26 July 2010; published 9 September 2010)

We find that in a multiorbital system, the Hall conductance may exhibit anomalous topological quantum phase transitions induced by on-site orbital polarization: both integer quantum-Hall (IQH) plateau transitions and topological-Fermi-liquid (TFL) to IQH transitions. The unusual TFL-to-IQH transitions are peculiar manifestations of orbital degeneracy and spatial anisotropy, and are demonstrated explicitly in a *p*-band spinless fermionic system and a *d*-band spinful fermionic system.

DOI: 10.1103/PhysRevB.82.113304 PACS number(s): 73.43.Nq, 03.75.Ss, 72.80.Ga, 73.43.Cd

I. INTRODUCTION

Recently, it is proposed that novel *p*-orbital physics, not realized in solid-state systems, may exist in optical lattices, and earlier attention has been paid on bosons in the first excited *p*-orbital bands.[1] Rapid experimental advances in loading and controlling alkali atoms on the excited bands makes the *p*-orbital physics truly fascinating.[2] Correlated fermions in the *p*-orbital bands possess more arresting behaviors, including Wigner crystallization, orbital ordering and frustration.[3] Even for noninteracting *p*-band fermions, nontrivial topological band structures arises from lifting the orbital degeneracy, and Haldane's model of quantum anomalous-Hall effect[4] can be realized.[5]

In parallel, for transition-metal oxides, the relevant active orbitals are the partially filled five *d* orbitals. Recently, giant spin-Hall and orbital-Hall effects have been found in transition metals and their compounds,[6] and many theoretical studies are based on realistic multiband 4*d* or 5*d* models.[7–9] A possible intrinsic origin of these giant Hall effects is the "orbital Aharonov-Bohm phase" which is induced by the atomic spin-orbital coupling (SOC) and the phase of interorbital hopping integrals characteristic of *d*-orbital systems.[7,8]

Given the intensive current interest in possible novel *p*-orbital and *d*-orbital physics which has not appeared in single-orbital systems, we are motivated to study magnetotransport properties of multiorbital fermions. We find that the Hall conductance (HC) may exhibit anomalous topological quantum phase transitions (QPTs) induced by on-site orbital polarization: integer quantum-Hall (IQH) plateau transitions and topological-Fermi-liquid (TFL) to IQH transitions. Such topological QPTs are demonstrated in two systems: a *p*-band spinless fermionic system which is proposed to be realized with ultracold atoms in optical lattice[5] and a *d*-band spinful fermionic system which is closely related to giant orbital-Hall effect in transition metals and their compounds.[7,8]

II. FORMULATION

The first model is a *p*-band system of p_x and p_y orbitals in a two-dimensional (2D) square lattice filled with spinless fermions coupled to an artificial uniform magnetic flux[3,5,10]

$$\begin{aligned} H_p = & \sum_{\mathbf{r}} \sum_{\mu,\nu=x,y} [t_{\parallel}\delta_{\mu\nu} - t_{\perp}(1-\delta_{\mu\nu})] \\ & \times [p^{\dagger}_{\mu,\mathbf{r}} p_{\mu,\mathbf{r}+\mathbf{e}_\nu} \exp(i\phi_{\mathbf{r},\mathbf{r}+\mathbf{e}_\nu}) + \text{H.c.}] \\ & + \lambda \sum_{\mathbf{r}} (ip^{\dagger}_{x,\mathbf{r}} p_{y,\mathbf{r}} - ip^{\dagger}_{y,\mathbf{r}} p_{x,\mathbf{r}}), \end{aligned} \tag{1}$$

where $p^{\dagger}_{\mu,\mathbf{r}}$ creates a fermion of $\mu=x,y$ *p* orbital at site $\mathbf{r}$. $t_{\parallel}$ ($t_{\perp}$) is the nearest-neighbor (NN) hopping integral in the longitudinal (transverse) direction to each *p*-orbital orientation. $t_{\parallel}, t_{\perp} > 0$, $t_{\perp}$ is one order of magnitude smaller than $t_{\parallel}$, and $t_{\parallel}$ will be taken as the unit of energy. A finite λ induces the rotation of each site around its own center, thus gives rise to orbital polarization by lifting the degeneracy between $p_x \pm ip_y$ orbitals.[5,10]

The second model is a *d*-band system of $d_{xz,\sigma}$ and $d_{yz,\sigma}$ orbitals (simplifying $d_{xz,\sigma} \equiv d_{x\sigma}$ and $d_{yz,\sigma} \equiv d_{y\sigma}$) in a 2D square lattice filled with spinful fermions[7,8]

$$\begin{aligned} H_d = & -t_{\parallel} \sum_{\mathbf{r},\sigma,\mu} [d^{\dagger}_{\mu\sigma,\mathbf{r}} d_{\mu\sigma,\mathbf{r}+\mathbf{e}_\mu} \exp(i\phi_{\mathbf{r},\mathbf{r}+\mathbf{e}_\mu}) + \text{H.c.}] \\ & + t' \sum_{\mathbf{r},\sigma} [d^{\dagger}_{x\sigma,\mathbf{r}} d_{y\sigma,\mathbf{r}\pm\mathbf{e}_x\pm\mathbf{e}_y} \exp(i\phi_{\mathbf{r},\mathbf{r}\pm\mathbf{e}_x\pm\mathbf{e}_y}) + \text{H.c.}] \\ & - t' \sum_{\mathbf{r},\sigma} [d^{\dagger}_{x\sigma,\mathbf{r}} d_{y\sigma,\mathbf{r}\pm\mathbf{e}_x\mp\mathbf{e}_y} \exp(i\phi_{\mathbf{r},\mathbf{r}\pm\mathbf{e}_x\mp\mathbf{e}_y}) + \text{H.c.}] \\ & + \lambda \sum_{\mathbf{r}} (id^{\dagger}_{x\downarrow,\mathbf{r}} d_{y\downarrow,\mathbf{r}} - id^{\dagger}_{x\uparrow,\mathbf{r}} d_{y\uparrow,\mathbf{r}} + \text{H.c.}), \end{aligned} \tag{2}$$

where $d^{\dagger}_{\mu\sigma,\mathbf{r}}$ creates a fermion of $\mu=xz,yz$ *d* orbital and spin $\sigma=\uparrow,\downarrow$ at site $\mathbf{r}$. $t_{\parallel}$ is the NN intraorbital hopping integral in the longitudinal direction and $\pm t'$ is the next NN interorbital hopping integrals. $t_{\parallel}, t' > 0$, and t' is one order of magnitude smaller than $t_{\parallel}$. Here λ is the atomic SOC strength.[7,8]

We consider $1/N$ magnetic flux quantum per plaquette (N is an integer), i.e., $\phi = \Sigma_{\square}\phi_{ij} = 2\pi Ba^2/\phi_0 = 2\pi/N$ with a the lattice constant and $\phi_0 = hc/e$ the flux quantum. The Landau gauge $\mathbf{A} = (0, -Bx, 0)$ and the periodical boundary conditions (PBCs) are adopted, and the magnetic unit cell has the size $Na \times a$. After the numerical diagonalization of the Hamiltonian, the zero-temperature HC is given by the Kubo formula[11]

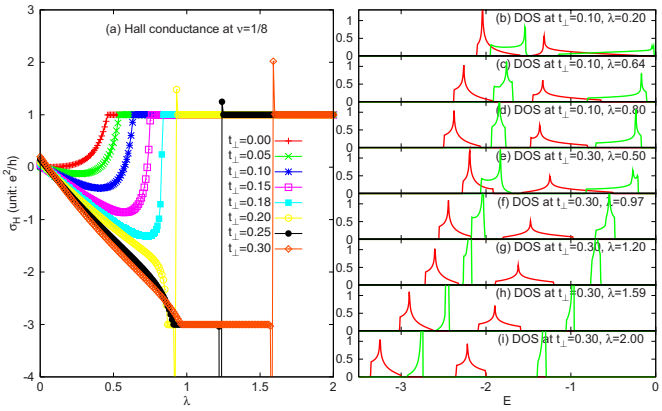

FIG. 1. (Color online) (a) Hall conductance versus λ (unit: $t_{\|}$) of p-band spinless fermions at $\nu=1/8$ with $N=4$ and various $t_{\perp}$'s. [(b)–(i)] The DOS for some $t_{\perp}$'s and λ's in (a).

$$\sigma_{\mathrm{H}}(E)=\frac{ie^2\hbar}{A}\sum_{\mathcal{E}_{n\mathbf{k}}<E}\sum_{\mathcal{E}_{m\mathbf{k}}>E}\times\frac{\langle n\mathbf{k}|v_x|m\mathbf{k}\rangle\langle m\mathbf{k}|v_y|n\mathbf{k}\rangle-\langle n\mathbf{k}|v_y|m\mathbf{k}\rangle\langle m\mathbf{k}|v_x|n\mathbf{k}\rangle}{(\mathcal{E}_{m\mathbf{k}}-\mathcal{E}_{n\mathbf{k}})^2} \tag{3}$$

with the system area $A=L\times L$, the Fermi energy E, the eigenvalue $\mathcal{E}_{n\mathbf{k}}$ and eigenstate $|n\mathbf{k}\rangle$ of nth Landau subband, and the summation over $\mathbf{k}$ is restricted to the magnetic Brillouin zone (MBZ): $-\pi/N\le k_x a<\pi/N$ and $-\pi\le k_y a<\pi$. The velocity operator is $\mathbf{v}=(i/\hbar)[H,\mathbf{R}]$ with $\mathbf{R}$ as the position operator of fermions. When E falling in energy gaps, we can rewrite σ_{H} as $\sigma_{\mathrm{H}}(E)=\Sigma_{\mathcal{E}_n<E}\sigma_{\mathrm{H}}^{(n)}=e^2/h\Sigma_{\mathcal{E}_n<E}C_n$, where $\sigma_{\mathrm{H}}^{(n)}$ and C_n are the HC and the Chern number (a topological invariant of the MBZ) (Ref. 11) of the nth completely filled subband, respectively. An IQH effect, characterized by nonzero Chern integers, is a Fermi sea property.

With the Berry connection $\mathbf{A}_n(\mathbf{k})=i\langle n\mathbf{k}|\nabla_{\mathbf{k}}|n\mathbf{k}\rangle$ and Berry curvature $\mathbf{\Omega}_n(\mathbf{k})=\nabla_{\mathbf{k}}\times\mathbf{A}_n(\mathbf{k})$ defined, the quantized HC of a completely filled nth subband can be written as $(h/e^2)\sigma_{\mathrm{H}}^{(n)}=(1/2\pi)\int\int_{\mathrm{MBZ}}\mathbf{\Omega}_n^z(\mathbf{k})d^2\mathbf{k}=(1/2\pi)\oint_{\mathrm{MBZ}}\mathbf{A}_n(\mathbf{k})\cdot d\mathbf{k}=\Gamma_{\mathrm{MBZ}}^{(n)}/2\pi$, where $\Gamma_{\mathrm{MBZ}}^{(n)}$ is the Berry's geometric phase factor of the cyclic evolution of $|n\mathbf{k}\rangle$ along the MBZ boundary.[11] For a partially filled nth subband, the nonquantized part of the HC can also be written as $(h/e^2)\sigma_{\mathrm{H}}^{(n)}=(1/2\pi)\oint_{\mathrm{FS}}\mathbf{A}_n(\mathbf{k})\cdot d\mathbf{k}=\Gamma_{\mathrm{FS}}^{(n)}/2\pi$, where $\Gamma_{\mathrm{FS}}^{(n)}$ is the Berry phase of the cyclic evolution of $|n\mathbf{k}\rangle$ along the Fermi surface (FS) and thus represents a TFL property.[12]

III. p-BAND SPINLESS FERMIONS

A. Hall conductances

An overall picture of the HC σ_{H} calculated by Eq. (3) is shown in Fig. 1 for p-band spinless fermions [Eq. (1)] with $N=4$ (i.e., the flux strength $\phi=\frac{1}{4}\times 2\pi$), 2048×2048 lattice sites, fermion filling $\nu=1/8$, and various $t_{\perp}$'s.

In the case of $\lambda=0$, the lowest two subbands (each contributes $\frac{1}{8}$ to ν) are not separated; they give rise to a total Chern number +2. With λ increasing from 0 to 2.0 one sees a systematic evolution of σ_{H} versus λ; for smaller $t_{\perp}$'s, there is a quantum-critical point (QCP) λ_{c1} at which the lowest two subbands begin to separate; for larger $t_{\perp}$'s, besides the first QCP λ_{c1}, there is another QCP λ_{c2} at which σ_{H} exhibits a quantized jump.

TABLE I. Topological QPTs of p-band spinless fermions.

$(N,\nu,t_{\perp})$	λ_{c1}	λ_{c2}	Quantized jump of σ_{H} at λ_{c2}
(6,1/12,0.25)	0.70	1.16	$-5e^2/h\rightarrow+1e^2/h$
(8,1/16,0.20)	0.50	0.89	$-7e^2/h\rightarrow+1e^2/h$
(8,3/16,0.25)	0.41	0.59	$-5e^2/h\rightarrow+3e^2/h$
(12,1/24,0.20)	0.42	0.92	$-11e^2/h\rightarrow+1e^2/h$
(12,3/24,0.20)	0.29	0.45	$-9e^2/h\rightarrow+3e^2/h$
(16,1/32,0.10)	0.24	0.44	$-15e^2/h\rightarrow+1e^2/h$
(16,3/32,0.20)	0.26	0.53	$-13e^2/h\rightarrow+3e^2/h$
(16,5/32,0.20)	0.20	0.26	$-11e^2/h\rightarrow+5e^2/h$

At smaller $t_{\perp}$'s ($t_{\perp}=0.00,\ldots,0.18$), for $\lambda>\lambda_{c1}$ (e.g., $\lambda_{c1}\simeq 0.64$ for $t_{\perp}=0.10$), the lowest two subbands are well separated since λ lifts the p-orbital degeneracy and induces a finite energy gap; the lowest subband is occupied by p_x+ip_y fermions while the second lowest one by p_x-ip_y fermions, each subband carrying a Chern number +1, and $\sigma_{\mathrm{H}}=+1e^2/h$ (i.e., $C_1=+1$) at $\nu=1/8$.

At larger $t_{\perp}$'s ($t_{\perp}=0.20,0.25,0.30$), for $\lambda>\lambda_{c1}$ (e.g., $\lambda_{c1}\simeq 0.97$ for $t_{\perp}=0.30$), the lowest two subbands are also well separated; however, the lowest subband occupied by p_x+ip_y fermions now gives a Chern number $C_1=-3$. When λ increases further to another QCP λ_{c2} (e.g., $\lambda_{c2}\simeq 1.59$ for $t_{\perp}=0.30$), σ_{H} exhibit a quantized jump from $-3e^2/h$ to $+1e^2/h$ at $\nu=1/8$ (i.e., C_1 changes from −3 to +1).

The above behaviors of HCs have also been verified by further numerical calculations of the cases with $N=6,\ldots,16$, various $t_{\perp}$'s and ν's (Table I).

B. Berry curvatures

In order to reveal the nontrivial topological properties in $\mathbf{k}$ space, we plot in Fig. 2 the sum of Berry curvatures over the occupied subbands, $\mathbf{\Omega}^z(\mathbf{k})=\Sigma_{\mathcal{E}_n<E}\mathbf{\Omega}_n^z(\mathbf{k})$, in the reduced MBZ (RMBZ) ($-\pi/N\le k_x a,k_y a<\pi/N$) for some typical parameters corresponding to Fig. 1.

We first look into the case of $t_{\perp}=0.1$ with only one λ_c (see Fig. 1). For $\lambda<\lambda_{c1}\simeq 0.64$, e.g., $\lambda=0.2$ [Fig. 2(a)], $\mathbf{\Omega}^z(\mathbf{k})$ displays the FS topology of two subbands: a hole FS of the lowest subband near four corners of the RMBZ and an fermion FS of the second lowest subband near the center of the RMBZ. There are four small negative-$\mathbf{\Omega}^z(\mathbf{k})$ regions near the hole FS. When λ increases, the two subbands starts to separate and two FSs shrinks gradually [Fig. 2(b)]. For $\lambda>\lambda_{c1}$, e.g., $\lambda=0.8$ [Fig. 2(c)], the two subbands separates completely, both FSs vanishes, and $\mathbf{\Omega}^z(\mathbf{k})$ displays four maxima (which contribute to $C_1=+1$) at the four RMBZ corners.

We then analyze the case of $t_{\perp}=0.3$ with two λ_c's (Fig. 1). For a small $\lambda=0.2$ [Fig. 2(d)], $\mathbf{\Omega}^z(\mathbf{k})$ also displays the FS topology of two subbands. $\mathbf{\Omega}^z(\mathbf{k})$ displays four negative regions between the hole and particle FSs. When λ increases,

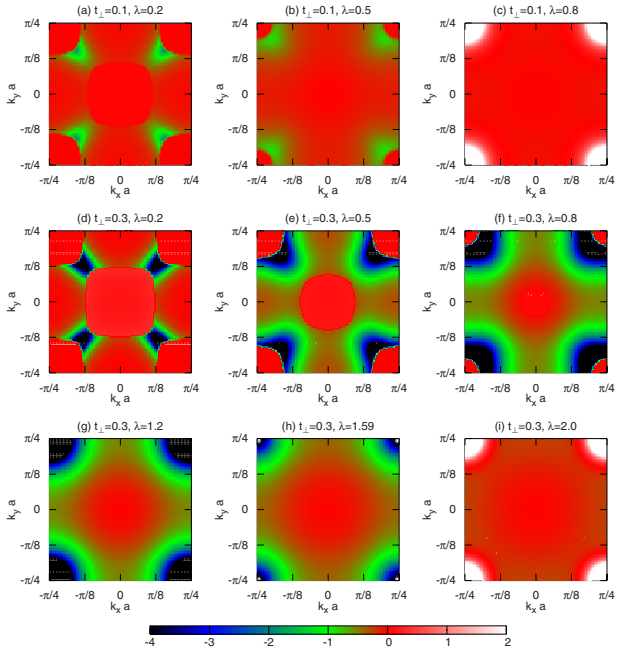

FIG. 2. (Color online) Intensity plots of Berry curvatures $\mathbf{\Omega}^z(\mathbf{k})$ in the RMBZ of p-band fermions at $\nu=1/8$ with $N=4$, various $t_\perp$'s and λ's.

e.g., $\lambda=0.5,0.8$ [Figs. 2(e) and 2(f)], negative-$\mathbf{\Omega}^z(\mathbf{k})$ regions also increase, change their topology, and enclose the four RMBZ corners, with the two FSs shrinking. When λ increases and passes $\lambda_{c1}=0.97$, e.g., $\lambda=1.2$ [Fig. 2(g)], the two subbands separates completely, and both FSs vanishes, and $\mathbf{\Omega}^z(\mathbf{k})$ displays four negative-$\mathbf{\Omega}^z(\mathbf{k})$ minima (which contribute to $C_1=-3$) at the four RMBZ corners. Near $\lambda_{c2}\simeq 1.59$ [Fig. 2(h)], four negative-$\mathbf{\Omega}^z(\mathbf{k})$ minima at the RMBZ corners begin to vanish. When λ increases further and passes λ_{c2}, e.g., $\lambda=2.0$ [Fig. 2(i)], the two subbands separates completely and four negative-$\mathbf{\Omega}^z(\mathbf{k})$ minima vanishes, and are replaced by positive-$\mathbf{\Omega}^z(\mathbf{k})$ maxima (which contribute to $C_1=+1$ again) at the RMBZ corners.

C. Edge states

An alternative way to reveal different topological characters and QPTs is to calculate the edge states.[13] Now as an illustration, we take a cylinder of square lattice of the size $64\times\infty$ with $N=4$ and $t_\perp=0.30$, and apply open boundary condition in x direction and PBC in y direction.

Chern numbers of the bulk subbands are intimately related to the winding numbers of the corresponding edge states.[13] We here concentrate on the edge states between the lowest two subbands shown in Fig. 3. For $0<\lambda<\lambda_{c1}\simeq 0.97$ (see the $t_\perp=0.30$ curve in Fig. 1), e.g., $\lambda=0.50$ [Fig. 3(a)], there is one edge state winding between the lowest two subbands, however, the Chern number of the lowest subband C_1 is not well defined since the energy overlap of the two subbands. For $\lambda_{c1}<\lambda<\lambda_{c2}\simeq 1.59$, e.g., $\lambda=1.20$ [Fig. 3(b)], there is one edge state winding three times from the lowest subband to the upper one then back to the lowest one which corresponds to $C_1=-3$. While $\lambda>\lambda_{c2}$, e.g., $\lambda=2.00$ [Fig. 3(d)], there is another edge state winding only once from the upper subband to the lowest one then back to the upper one which corresponds to $C_1=+1$.

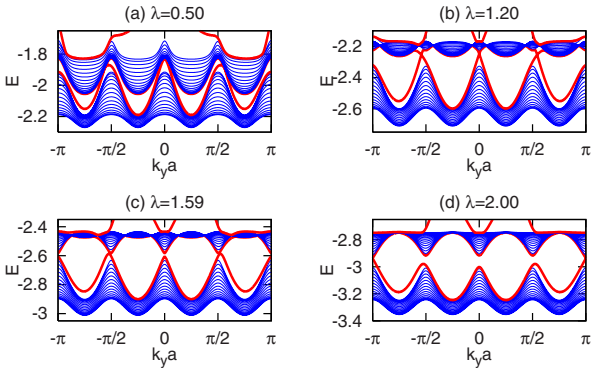

FIG. 3. (Color online) $E(k_y)$ of lowest two subbands and edge states [shown as thick (red) lines] of p-band fermions in a $64\times\infty$ cylinder with $t_\perp=0.30$ and various λ's.

There is also a correspondence between the quantized jumps of σ_H and the topological evolutions of bulk spectra.[4,14,15] When approaching λ_{c2}, four pairs of Dirac cones begin to form between the lowest two subbands and each pair touch at one Dirac point when $\lambda_{c2}\simeq 1.59$ [Fig. 3(c)]. Meanwhile, a topological QPT happens at λ_{c2}, and a Chern number +4 is transferred from the upper subband to the lowest one, through abrupt changes of Berry curvatures near Dirac points [Fig. 2(h)]. On contrary, at the first QCP $\lambda_{c1}\simeq 0.97$, there is no Dirac point, and thus no quantized jumps of σ_H.

IV. d-BAND SPINFUL FERMIONS

For d-band fermions [Eq. (2)] with additional spin degree of freedom, some typical examples of the HC σ_H calculated by Eq. (3) are shown in Fig. 4 for various N's, ν's and t''s. We note that TFL-to-IQH transitions occur rather frequently when tuning λ to critical values λ_c's. Since now we have two spin components, σ_H may change either $2Ne^2/h$ [e.g., the $t'=0.3$ case in Fig. 4(a)] or Ne^2/h [e.g., the $t'=0.4$ case in Fig. 4(c)], after passing a TFL region or a quantized jump. And we numerically confirmed that such topological QPTs are also reflected in both Berry curvatures and edge states.

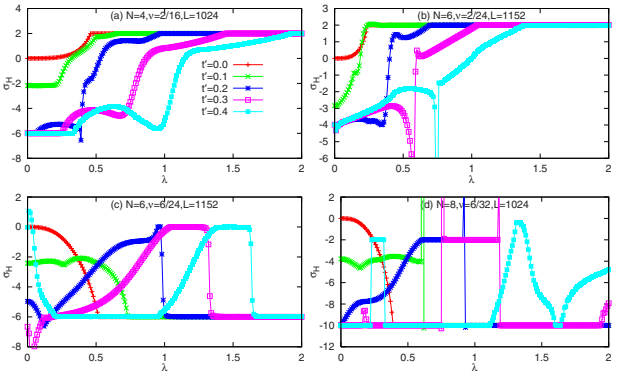

FIG. 4. (Color online) σ_H (unit: e^2/h) versus λ (unit: $t_\parallel$) of d-band spinful fermions at various N's, ν's and t''s.

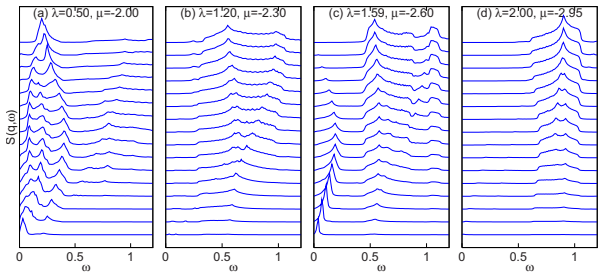

FIG. 5. (Color online) $S(\mathbf{q},\omega)$ versus ω of p-band fermions, at various $q_y a = l\pi/32$ ($l=1,\ldots,16$ from bottom to top). [(a)–(d)] correspond to Figs. 3(a)–3(d), respectively.

V. EXPERIMENTAL ISSUES

The required artificial magnetic flux in optical lattices is suggested to be created by laser assisted tunneling between internal atomic states or time-varying quadrupole potential[16] and is feasible as shown by recent experimental advances.[17] The rotation of each optical lattice site around its own site center has been performed via electro-optic phase modulation on laser beams[18] and, in principle, can give rise to a tunable orbital polarization.[5]

The direct detection of topological states through transport measurement in cold atom experiments might be difficult. The Bragg spectroscopy provides a direct experimental probe to detect the topological phase transitions[19] by shining two lasers on the whole lattice system including two edges. This light Bragg scattering directly measures the following dynamical structure factor: $S(\mathbf{q},\omega) = \Sigma_{\mathbf{k}_1,\mathbf{k}_2} |\langle \mathrm{fin},\mathbf{k}_2|H_{\mathrm{int}}|\mathrm{ini},\mathbf{k}_1\rangle|^2 \delta(\hbar\omega - E^{\mathrm{fin}}_{\mathbf{k}_2} + E^{\mathrm{ini}}_{\mathbf{k}_1})$, where $H_{\mathrm{int}} = \Sigma_{\mathbf{k}_1,\mathbf{k}_2} \Omega e^{i\mathbf{q}\cdot\mathbf{r}} |\mathrm{ini},\mathbf{k}_1\rangle\langle \mathrm{fin},\mathbf{k}_2| + \mathrm{H.c.}$ and the momentum transfer and energy transfer between initial and final states are related to the two laser beams (with $\mathbf{k}_{1,2}$ and $\omega_{1,2}$) as $\mathbf{q}=\mathbf{k}_2-\mathbf{k}_1$ and $\omega=\omega_2-\omega_1$. For the same cylinder system of Fig. 3, $S(\mathbf{q},\omega)$ indeed tell distinct features among topological and critical phases. The multipeak structure near low frequency appears for TFL with overlapping subbands [Fig. 5(a)]. Both the low-frequency cutoffs of Figs. 5(b) and 5(d) state that the system is in the IQH phases. And the low-frequency single peak is a characteristic feature of a QCP [Fig. 5(c)].

VI. SUMMARY AND CONCLUSION

We show that in a multiorbital system with intraorbital and interorbital hopping integrals, the HC may exhibit both IQH-to-IQH transitions and anomalous TFL-to-IQH transitions induced by on-site orbital polarization. Berry curvatures, edge states, and Bragg spectroscopy give further insights to reveal various topological characters. The IQH-to-IQH transitions also occur in single orbital systems and are always accompanied by changes in Chern numbers; while the unusual TFL-to-IQH transitions, not accompanied by the changes in Chern numbers, but due to the evolutions of Berry curvatures and Fermi surfaces of overlapping subbands, are peculiar manifestations of orbital degeneracy and spatial anisotropy.

ACKNOWLEDGMENTS

This work was supported by the National Natural Science Foundation of China (Grant No. 10904130), and the State Key Program for Basic Researches of China (Grants No. 2006CB921802 and No. 2009CB929504).

[1] A. Isacsson and S. M. Girvin, Phys. Rev. A **72**, 053604 (2005); W. V. Liu and C. Wu, *ibid.* **74**, 013607 (2006); A. B. Kuklov, Phys. Rev. Lett. **97**, 110405 (2006); C. Wu, W. V. Liu, J. E. Moore, and S. Das Sarma, *ibid.* **97**, 190406 (2006).

[2] M. Köhl, H. Moritz, T. Stöferle, K. Günter, and T. Esslinger, Phys. Rev. Lett. **94**, 080403 (2005); T. Müller, S. Fölling, A. Widera, and I. Bloch, *ibid.* **99**, 200405 (2007); M. Anderlini *et al.*, Nature (London) **448**, 452 (2007).

[3] C. Wu, D. Bergman, L. Balents, and S. Das Sarma, Phys. Rev. Lett. **99**, 070401 (2007); C. Wu, *ibid.* **100**, 200406 (2008); E. Zhao and W. V. Liu, *ibid.* **100**, 160403 (2008).

[4] F. D. M. Haldane, Phys. Rev. Lett. **61**, 2015 (1988).

[5] C. Wu, Phys. Rev. Lett. **101**, 186807 (2008).

[6] S. O. Valenzuela and M. Tinkham, Nature (London) **442**, 176 (2006); N. P. Stern, S. Ghosh, G. Xiang, M. Zhu, N. Samarth, and D. D. Awschalom, Phys. Rev. Lett. **97**, 126603 (2006); T. Kimura, Y. Otani, T. Sato, S. Takahashi, and S. Maekawa, *ibid.* **98**, 156601 (2007).

[7] H. Kontani, T. Tanaka, D. S. Hirashima, K. Yamada, and J. Inoue, Phys. Rev. Lett. **100**, 096601 (2008); **102**, 016601 (2009).

[8] T. Tanaka, H. Kontani, M. Naito, T. Naito, D. S. Hirashima, K. Yamada, and J. Inoue, Phys. Rev. B **77**, 165117 (2008); T. Tanaka and H. Kontani, *ibid.* **77**, 195129 (2008).

[9] G. Y. Guo, S. Murakami, T. W. Chen, and N. Nagaosa, Phys. Rev. Lett. **100**, 096401 (2008).

[10] R. O. Umucalılar and M. Ö. Oktel, Phys. Rev. A **78**, 033602 (2008).

[11] D. J. Thouless, M. Kohmoto, M. P. Nightingale, and M. den Nijs, Phys. Rev. Lett. **49**, 405 (1982).

[12] F. D. M. Haldane, Phys. Rev. Lett. **93**, 206602 (2004).

[13] Y. Hatsugai, Phys. Rev. Lett. **71**, 3697 (1993).

[14] Y. Hatsugai and M. Kohmoto, Phys. Rev. B **42**, 8282 (1990).

[15] Y. F. Wang and C. D. Gong, Phys. Rev. Lett. **98**, 096802 (2007); Y. F. Wang, Y. Zhao, and C. D. Gong, Phys. Rev. B **78**, 045301 (2008).

[16] D. Jaksch and P. Zoller, New J. Phys. **5**, 56 (2003); A. S. Sørensen, E. Demler, and M. D. Lukin, Phys. Rev. Lett. **94**, 086803 (2005).

[17] Y. J. Lin, R. L. Compton, A. R. Perry, W. D. Phillips, J. V. Porto, and I. B. Spielman, Phys. Rev. Lett. **102**, 130401 (2009); Nature (London) **462**, 628 (2009).

[18] N. Gemelke, Ph.D. thesis, Stanford University, 2007.

[19] D. M. Stamper-Kurn, A. P. Chikkatur, A. Gorlitz, S. Inouye, S. Gupta, D. E. Pritchard, and W. Ketterle, Phys. Rev. Lett. **83**, 2876 (1999); S. L. Zhu, B. Wang, and L. M. Duan, *ibid.* **98**, 260402 (2007); X. J. Liu, X. Liu, C. Wu, and J. Sinova, Phys. Rev. A **81**, 033622 (2010).